Eur. Phys. J. B **18**, 329–335 (2000)

THE EUROPEAN PHYSICAL JOURNAL B

EDP Sciences

Statics and dynamics of a single ferrofluid-peak

R. Friedrichs[a] and A. Engel

FNW/ITP, "Otto-von-Guericke-Universität", Postfach 4120, 39016 Magdeburg, Germany

Received 14 December 1999 and Received in final form 31 May 2000

Abstract. We consider a single peak of a ferrofluid resulting from the Rosensweig instability for a small fluid container. Minimizing the total energy of the system by a variational method we determine the shape of the peak in a static field as well as the characteristics of the subcritical bifurcation leading to its formation. The latter are in very good agreement with experiment. Generalizing the approach to dynamic situations we qualitatively reproduce the complicated subharmonic response of the peak to an oscillating part in the external magnetic field found in recent experiments.

PACS. 47.20.Ky Nonlinearity (including bifurcation theory) – 47.20.Ma Interfacial instability – 75.50.Mm Magnetic liquids

1 Introduction

Ferrofluids are colloidal suspensions of ferromagnetic particles in a nonmagnetic carrier liquid. Due to the small size of about 10 nm the particles are magnetic monodomains and the fluids behave like super-paramagnetic materials [1,2]. The interaction between the magnetizable fluid and an external magnetic field gives rise to several interesting phenomena like new or modified instabilities [3], field depending viscosities [4,5], new dissipation mechanisms [6], and viscoelastic effects [7]. The possibility to modulate the hydrodynamic parameters of the fluid with an external magnetic field also opens the way for a variety of technical and medical applications [8].

In the present paper we investigate in detail the response of a ferrofluid surface with small horizontal extension on a static and time dependent vertical magnetic field, a situation which was studied in recent experiments [9]. As a consequence of the Rosensweig (or normal field) instability [10] a peak appears on the surface of the liquid. Previous theoretical investigations of this instability have been focused on the two-dimensional patterns [11,12] and the hysteretic behavior [13,14] of the peak formation. Extending these studies we also investigate the detailed *shape* of an individual peak. An analysis of this shape has been accomplished recently by means of a perturbation theory for the *one-dimensional* case [15]. Here we consider the more realistic but also more complicated case of a two-dimensional surface which cannot be investigated using a generalization of the methods used in the one-dimensional situation. Moreover, motivated by the wide spectrum of fascinating effects detected in different experiments [9,16,17] we study for the first time theoretically the *dynamic* behavior of a ferrofluid peak under the influence of an oscillating magnetic field.

The paper is organized as follows. In the next section we introduce the variational principle for the energy and discuss our parameterization of the peak shape. In Section 3, the magnetic field equations are transformed into a form suitable for the implementation into the variational calculation. Section 4 contains the results for the static situation with time independent field. Sections 5 and 6 specify the generalization of the model to dynamics and discuss the results for the case of an oscillating part in the magnetic field respectively. The last section gives a short summary and considers possible extensions of the present work.

2 Energy variational principle

We consider the axisymmetric situation sketched in Figure 1. A ferrofluid of density ρ, surface tension σ, and susceptibility χ is subject to an external field $\mathbf{H}_0$ which is in the absence of any magnetic material of the form

$$\mathbf{H}_0 = H_0 \mathbf{e}_z. \tag{1}$$

The gravitational acceleration $\mathbf{g} = -g\mathbf{e}_z$ is parallel to the z-axis. This setup was realized experimentally in [9]. The parameters are chosen such that the critical wavelength $\lambda_c = 2\pi\sqrt{\sigma/\rho g}$ of the Rosensweig instability [10] is larger than the diameter of the vessel. This gives rise to the formation of a single axisymmetric peak. The complete surface of the ferrofluid including the part inside the vessel is described by $\mathbf{S}(s) = (r(s)\cos(\phi), r(s)\sin(\phi), z(s))$ parameterized by a single scalar parameter s. Our aim is to determine the static free surface $\mathbf{S}_{\text{free}}(s)$ of the fluid between the contact points marked with the two black points

[a] e-mail: rene.friedrichs@physik.uni-magdeburg.de

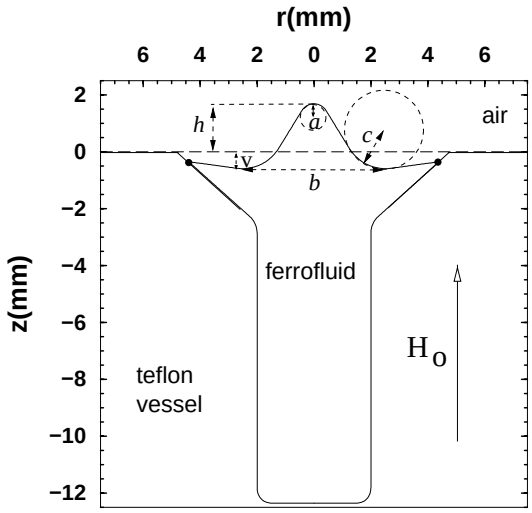

Fig. 1. Cylindrical Teflon vessel filled with ferrofluid in an external magnetic field $\mathbf{H}_0$ parallel to the z-axis. We investigate the profile of the free surface characterized by the parameters a, b, c, h and v.

in Figure 1. These points were found not to move in the experiment.

The static profile of the ferrofluid is the minimum of the thermodynamic potential

$$\tilde{F} = \rho g \int\limits_{V_{\rm ff}} \mathrm{d}V z + \sigma \oint\limits_{S_{\rm free}} \mathrm{d}S - \frac{\mu_0}{2} \int\limits_{V_{\rm ff}} \mathrm{d}V\, \mathbf{H}_0(\mathbf{r})\mathbf{M}(\mathbf{r}). \quad (2)$$

The first term in equation (2) is the hydrostatic energy, the second is the surface energy and the third is the magnetic energy [18], where μ_0 denotes the permeability of free space and $V_{\rm ff}$ the volume of the ferrofluid. The direct minimization of $\tilde{F}[\mathbf{S}_{\rm free}(s)]$ as a functional of the free surface is very difficult, in particular since the magnetic field for a given shape of the ferrofluid can only be determined numerically. Therefore we use a parameterization of the free surface profile as sketched in Figure 1 using as parameters the radius of curvature of the peak a, the diameter of the cone b, the radius of curvature of the dip c, and the height of the peak h and minimize $\tilde{F}$ with respect to these parameters. To this end the magnetization $\mathbf{M}(\mathbf{r})$ has to be calculated for each combination of the four parameters. Note that the depth of the dip v is not a free parameter since it is fixed by volume conservation.

3 Field equations

The axisymmetric magnetic field is determined by the static Maxwell equations

$$\nabla \cdot \mathbf{B} = 0 \quad \text{and} \quad \nabla \times \mathbf{H} = 0 \quad (3)$$

together with the conditions

$$\lim_{r\to\infty} \mathbf{H}(r,z) = H_0 \mathbf{e}_z = \lim_{z\to\infty} \mathbf{H}(r,z). \quad (4)$$

The magnetic fields used in the considered experiments are small enough to warrant the use of the linear relation

$$\mathbf{B} = \mu_0(\mathbf{H} + \mathbf{M}) = \mu_0(1+\chi)\mathbf{H} \quad (5)$$

between the magnetic induction and the magnetic field. The scalar magnetic potential $\psi(r,z)$ defined by

$$\mathbf{H} = -\nabla\psi \quad (6)$$

has then to satisfy the Laplace equation

$$\Delta\psi = 0 \quad (7)$$

inside and outside the ferrofluid. The ansatz

$$\psi(\mathbf{r}) = -H_0 z + \frac{1}{4\pi} \oint\limits_{\partial V_{\rm ff}} \mathrm{d}S\, \frac{q(\mathbf{s})}{|\mathbf{r}-\mathbf{s}|} \quad (8)$$

fulfills equation (7) and the condition equation (4). Here $\partial V_{\rm ff}$ denotes the surface of the ferrofluid. Also the tangential component of the field $\mathbf{H}$ is continuous at the ferrofluid surface. The introduced surface charge $q(\mathbf{s})$ is the source density of the magnetic field $\mathbf{H}$ and determined by the boundary condition

$$H_{\rm n}^{\rm out} = (1+\chi) H_{\rm n}^{\rm in}, \quad (9)$$

where $H_{\rm n}^{\rm out}$ and $H_{\rm n}^{\rm in}$ denote the normal component of the magnetic field outside and inside the ferrofluid, respectively. In this way the determination of the magnetic field can be reduced to the solution of the integral equation

$$\frac{2\chi}{\chi+2}\left[\frac{1}{4\pi} \oint\limits_{\partial V_{\rm ff}} \mathrm{d}S\, \frac{(\mathbf{r}-\mathbf{s})}{|\mathbf{r}-\mathbf{s}|^3}\mathbf{n}(\mathbf{r})q(\mathbf{s}) \;+\; H_0 \mathbf{e}_z \mathbf{n}(\mathbf{r})\right] = q(\mathbf{r}) \quad (10)$$

for the charge q on the fluid surface as introduced in equation (8). The normal vector $\mathbf{n}$ on the interface points to the outside of the fluid.

Exploiting the rotational symmetry of the problem (10) may be simplified to an inhomogeneous Fredholm equation of the second kind of the form

$$\int\limits_a^b \mathrm{d}s' K(s,s')\, Q(s') \;-\; 2H_0 \partial_s r(s) = \frac{\chi+2}{\chi} Q(s) \quad (11)$$

for the function

$$Q(s) := q(s)\sqrt{(\partial_s z(s))^2 + (\partial_s r(s))^2}. \quad (12)$$

The kernel $K(s,s') := \frac{r(s')}{\pi} \int\limits_0^\pi \mathrm{d}\phi \times$

$$\frac{\partial_s z(s)\,(r(s) - r(s')\cos\phi) - \partial_s r(s)\,(z(s) - z(s'))}{\left(\sqrt{r^2(s) - 2r(s)r(s')\cos\phi + r^2(s') + (z(s)-z(s'))^2}\right)^3} \quad (13)$$

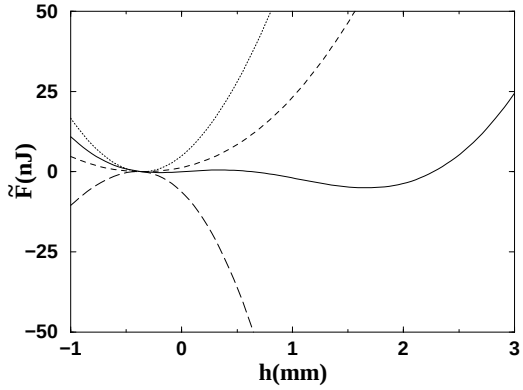

Fig. 2. The thermodynamic potential $\tilde{F}$ (full line) as the sum of the hydrostatic energy (dashed), the surface energy (dotted) and the magnetic energy at $H_0 = 0.97H_c$ (long-dashed) as function of the height h of the peak. The parameters of the considered ferrofluid are listed in equations (14).

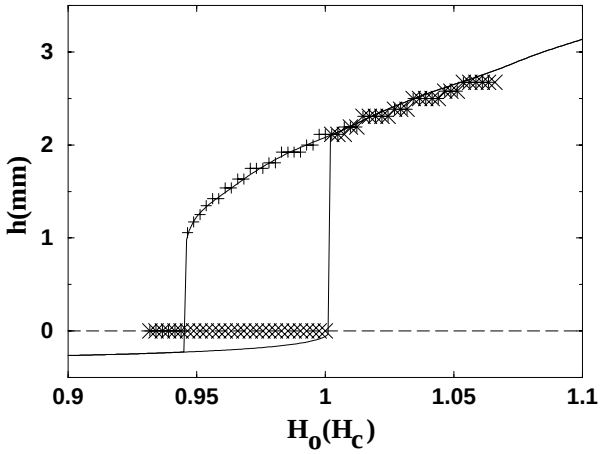

Fig. 3. Height of the peak h *versus* the strength of the static field H_0. The crosses mark the experimental data for increasing ($\times$) and decreasing field($+$). The full line represents our theoretical results for the hysteresis. In the experiment [9] negative heights could not been measured and were considered to be zero.

is quite complicated and therefore equation (11) is solved by discretizing s and solving numerically the corresponding linear equations. We note that the diagonal elements of the corresponding matrix $K_{s,s'}$ are not singular except for the singularity induced by the infinite curvature of the surface at the contact points (*cf.* Fig. 1). In these regions a finer discretisation was used, which had to be readjusted for each profile in order to achieve accurate results for the surface charge $q(s)$ and the corresponding magnetic potential $\psi(r, z)$ with reasonable numerical effort.

4 The static behavior

Using the methods explained in the previous section to determine the magnetic field for a time-independent external field the thermodynamic potential $\tilde{F}(a, b, c, h)$ may be calculated for different values of the parameters corresponding to different shapes of the ferrofluid peak. We then minimize $\tilde{F}$ numerically with respect to all four parameters to obtain the equilibrium configuration of the free surface. For the hydrodynamic parameters we used the experimentally relevant values [19]

$$\rho g = 1.35 \times 10^4 \text{ kg m}^{-2} \text{ s}^{-2},\ \sigma = 2.05 \times 10^{-2} \text{ kg s}^{-2},$$
$$\chi = 2.93 \qquad (14)$$

where σ and χ were fitted to the values of the critical field H_c and the saddle-node field H_s (see below). We note that the surface tensions changes with temperature and the susceptibility increases due to aging effects.

It turns out that the values of a, b, and c at the minimum of $\tilde{F}$ hardly depend on the external magnetic field H_0. In the following they will therefore be fixed to the values $a_{\min} = 0.5$ mm, $b_{\min} = 3.5$ mm, and $c_{\min} = 1.5$ mm respectively.

In Figure 2 we have plotted the thermodynamic potential $\tilde{F}(a_{\min}, b_{\min}, c_{\min}, h)$ as a function of the height of the peak h. This function and the position of its minimum strongly depends on the magnetic field H_0. For a certain range of the field strength the potential has two local minima pointing to a backward bifurcation with hysteresis. We denote by H_c the critical field for the onset of the instability and by H_s the saddle-node field for the collapse of the peak. In the experiment described in [9] they have been measured to be $H_c = 6.2 \times 10^3 \text{A m}^{-1}$ and $H_s = 5.8 \times 10^3 \text{A m}^{-1}$.

Figure 3 shows the measured and the calculated height h of the peak as function of the external field H_0 measured in units of H_c. Note that only σ and χ have been fitted by comparing the therewith calculated H_c and H_s with the experimentally observed values. The very good agreement of the calculated *heights* of the peak with the measured values therefore validates our model parameterization. The height of the peak at onset is 2.1 mm, whereas shortly before the disappearance of the peak after reducing the field down to $H_s = 0.94H_c$ the height is 1.0 mm.

The shape of the ferrofluid surface with the theoretically determined values of a, b, c and h for the upper branch in Figure 3 at $H = 0.97H_c$ is shown in Figure 1.

5 Modelling the dynamics

The dynamics of the ferrofluid peak in the domain of the subcritical bifurcation was investigated experimentally [9] by means of an oscillating magnetic field of the form

$$H(t) = H_0 + \Delta H \sin(2\pi t f_D), \qquad (15)$$

with a static part H_0 and an oscillating part with amplitude ΔH. The oscillations of the ferrofluid peak were analyzed and the response period T was compared with the period of the driving magnetic field T_D at different driving frequencies f_D. For given H_0 the measurements were restricted to those values of ΔH for which the peak disappeared at least once during its oscillation cycle.

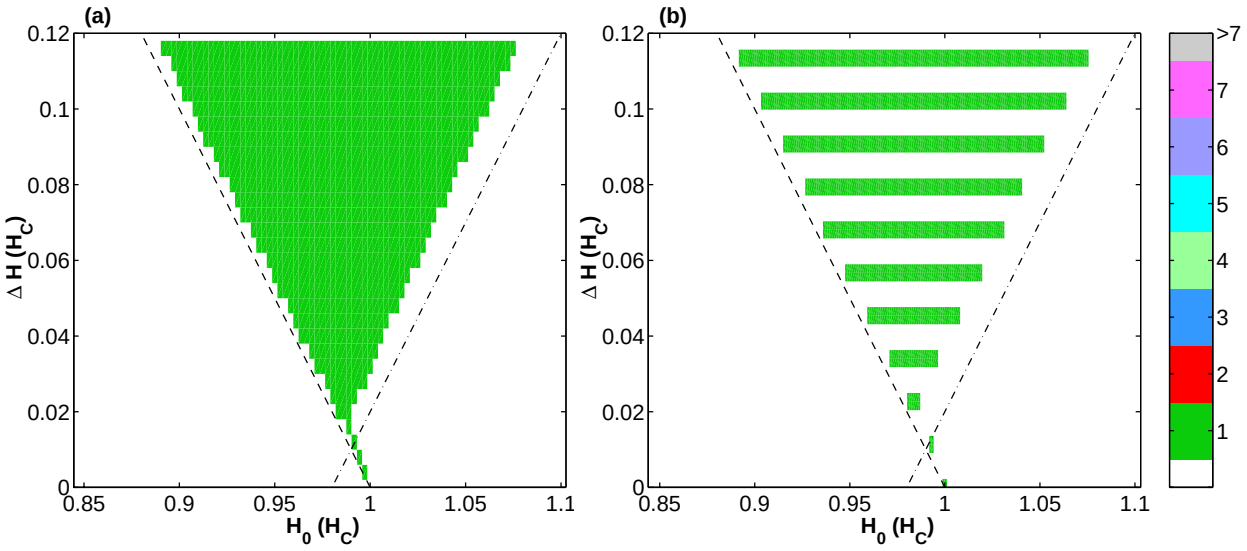

Fig. 4. Period T of the peak oscillations in units of the driving period T_D as function of the static field H_0 and the alternating field ΔH. For low driving frequency $f_\mathrm{D} = 2.5$ Hz both in our simulation (a) and in the experiment (b) only a harmonic response is observed. The dashed line $\Delta H = H_\mathrm{c} - H_0$ and the dashed-dotted line $\Delta H = H_0 - H_\mathrm{s}$ mark the limits in the quasistatic case. The higher value of the critical field $H_\mathrm{c} = 6.6 \times 10^3 \mathrm{A\,m^{-1}}$ measured in the experiment indicates that χ was lower then the susceptibility in the static case. By fitting this new H_c the corresponding value of $\chi = 2.39$ was determined. Simultaneously the saddle-node field $H_\mathrm{s} = 0.98 H_\mathrm{c}$ gets closer to the critical field. This second effect of a lower susceptibility is reproduced exactly by our calculations without fitting σ.

We model the dynamics of the ferrofluid peak on the basis of the thermodynamic potential $\tilde{F}$, which we have already calculated before. Assuming that the radius of curvature of the peak a, the diameter of the cone b and the radius of curvature of the dip c do not change during the oscillations we use the differential equation

$$m\ddot{h} + \frac{m}{\tau}\dot{h} = -\partial_h \tilde{F}(h; H(t)) \qquad (16)$$

for the time dependence of the height of the peak $h(t)$. Here a dot denotes the derivative with respect to time. The right hand side of equation (16) represents the force on the peak and varies with the time due to the dependence of the thermodynamic potential $\tilde{F}(h; H(t))$ on the oscillating magnetic field. On the left hand side the influences of inertia and the damping are modeled in a phenomenological manner. Note that a more detailed account for these effects would necessitate a complete analysis of the flow field inside the ferrofluid which is rather complicated. The parameters $m = 3.61 \times 10^{-3}$ g and $\tau = 13.4 \times 10^{-3}$ s were determined by fitting the dynamics resulting from equation (16) to the oscillations observed in the experiment. The value found for m is equivalent to a volume of 2.62 mm^3 of the used ferrofluid, which is reasonable. Also τ is in the order of the experimentally determined characteristic time of the system $\Theta = 40 \times 10^{-3}$ s, which is given by the decay time of the peak if the field is suddenly turned off.

In contrast to the left hand side of equation (16) the force $-\partial_h \tilde{F}(h)$ is nonlinear in h as can be seen from Figure 2. We solve equation (16) numerically by means of the fourth-order Runge-Kutta integration method with a time step of $T_\mathrm{D}/50$. To ensure that our results are independent of the chosen initial conditions $h(0) = -0.35$ mm and $\dot{h}(0) = 0\ \mathrm{mm\,s^{-1}}$ we calculate the solution over a total time of 107 T_D and analyse the last 7 periods with respect to a periodic behavior of $h(t)$. The period of the peak oscillations $h(t)$ is determined by means of Poincaré sections. Since we use a one-dimensional second order differential equation to model the dynamics of the ferrofluid we compare $h(100T_\mathrm{D})$ and $\dot{h}(100T_\mathrm{D})$ with $h(100T_\mathrm{D}+nT_\mathrm{D})$ and $\dot{h}(100T_\mathrm{D}+nT_\mathrm{D})$, respectively, for $n \in \{1, 2, ..., 7\}$. The smallest n with equality in both h and $\dot{h}$ gives the period time of the peak oscillations $T = nT_\mathrm{D}$ in units of the driving period.

6 Results and discussion

The dependence of the oscillation period T of the ferrofluid peak on the static field H_0 and on the oscillating part ΔH is shown in Figures 4a, 5a, 7a for three different driving frequencies f_D. For 90×30 points in the $H_0 \times \Delta H$ plane the oscillation periods were determined and displayed by different colors. To facilitate the comparison the experimental findings [9] are also shown. The harmonic response is represented by the green color, a subharmonic response with a period of $T = 2T_\mathrm{D}$ by red. If the period time is longer then $7T_\mathrm{D}$ the point in the diagram is marked gray indicating that the peak oscillates with a higher period or that chaotic dynamics may be observed. In the experiments the period T was determined when a tip of ferrofluid could be observed, *i.e.* the tip was higher than the edge of the vessel, and the peak collapsed completely at least

once during its oscillations. The same criterion giving rise to the borderlines of the colored regions was used in displaying the theoretical results. The relation between the borderlines in both plots may hence serve as a first hint on how well theoretical and experimental results coincide.

6.1 Low frequency

Our results for low driving frequency $f_\mathrm{D} = 2.5$ Hz are shown in Figure 4a. They agree rather well with the experimental data displayed in Figure 4b. The cone like shaped region is completely green colored since only a harmonic response is observed. The boundaries of the cone may be understood from the quasistatic limit $f_\mathrm{D} \to 0$. Then a peak should arise if the driving magnetic field $H(t)$ exceeds the critical field H_c at some time and collapse if the driving magnetic field $H(t)$ gets smaller then the saddle-node field H_s for another time. Therefore the period of the peak oscillations should be displayed only in the upper sector limited by the dashed line $\Delta H = H_\mathrm{c} - H_0$ and the dashed-dotted line $\Delta H = H_0 - H_\mathrm{s}$. As the results show already for driving frequency $f_\mathrm{D} = 2.5$ Hz both in our theory and in the experiment two deviations from this quasistatic behavior can be observed. Firstly, the right border of the area, in which the peak does not break down, is shifted to the left. This shift can be explained by the fact that for a magnetic field $H = (H_\mathrm{s} + H_\mathrm{c})/2$ in the middle of the hysteresis the global minimum of the thermodynamic potential $\tilde{F}(h, H)$ at the larger peak height h is more pronounced then the local minimum at the nearly flat surface as can be seen in Figure 2. Hence an oscillation of the peak around the larger height is more likely then a collapse of the peak. Secondly, for small amplitudes of the driving field occurs a slight asymmetry of the shape in the $H_0 - \Delta H$ plane develops and the peak breaks down although the total field is always larger than H_s. This effect points to the relevance of the inertial term in (16) which allows the system to overcome the barrier of the thermodynamic potential and to reach the local minimum at $h < 0$.

6.2 Medium frequency

Also for peak oscillations excited with a medium frequency of $f_\mathrm{D} = 13$ Hz good agreement between theory and experiment is found as shown in Figure 5. The shapes of the colored regions roughly coincide and also the internal transition lines are qualitatively reproduced by the theoretical results. For low values of H_0 the surface response is harmonic. A subharmonic response with $T = 2T_\mathrm{D}$ can be observed in the upper regions of the two period maps. Both of this red areas form two tongues, which extend to lower regions of the map, with the tongues even reaching the bottom of the colored region in the experimental data. In the ΔH-range from about $0.1H_\mathrm{c}$ to $0.2H_\mathrm{c}$ a domain of oscillations with a period time $T \geq 3T_\mathrm{D}$ is observed. The period-3-state is surrounded by a band of intermittent states, which is wider for large amplitudes of the driving field ΔH. While a period-1-state softly bifurcates into a period-2-state, there exists no smooth transition from $T = 1T_\mathrm{D}$ or $T = 2T_\mathrm{D}$ to $T = 3T_\mathrm{D}$ and we observe the same irregular change of the dynamics between these attractors as in the experiment. Even oscillations with the subharmonic modes $4, 5, 6$ and 7 can be found.

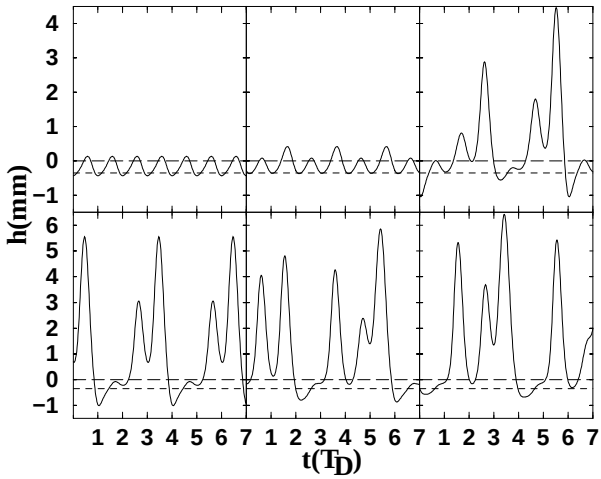

Fig. 6. The simulated oscillations of the peak height during 7 periods of excitation for six different dimensionless static field values $H_0 = 0.975, 1.025, 1.038, 1.075, 1.090$ and 1.125 at medium frequency $f_\mathrm{D} = 13$ Hz and fixed amplitude of the alternating field $\Delta H = 0.184 H_\mathrm{c}$. The long dashed line is indicating the edge of the vessel and the dashed line the flat surface. The corresponding surface response takes place with period 1, period 2, intermittency, period 3, period 7 and intermittency, respectively. Note that peaks not crossing the long-dashed line were not seen in the experiment.

For medium frequency we also display the detailed time behavior as shown in Figure 6. The transition from the period-1 and the period-2-state to the intermittent state is accompanied by strong variations in the amplitude of the oscillations, a peculiarity also seen in the experiments.

6.3 High frequency

Figure 7 shows the results for the high driving frequency $f_\mathrm{D} = 23.5$ Hz. In our period map (a) only oscillation with the period time $T = 1T_\mathrm{D}$ and $T = 2T_\mathrm{D}$ show up, whereas in the experiment (b) also higher periods and chaotic dynamics were observed. Moreover the calculated band with the harmonic response is wider then the measured one with, however, their progressions agreeing. In our simulation and in the experiments at $\Delta H = 0.3$ and $\Delta H = 0.2$, respectively, a period-2-state for a large range of the static magnetic field H_0 occurs. Generally speaking the agreement between theory and experiment is less convincing than in the previous cases indicating that with increasing frequency the applicability of our simple phenomenological model (16) of the peak dynamics gets questionable. A much more complicated treatment including the whole hydrodynamics of the ferrofluid is likely to be necessary for a thorough understanding of this high frequency domain.

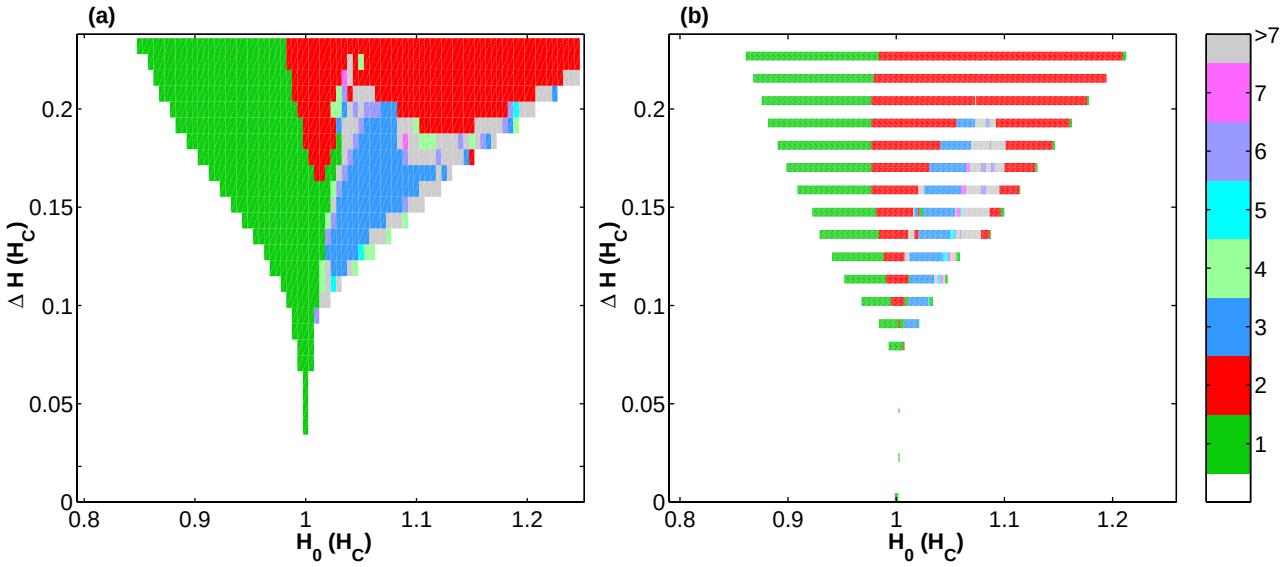

Fig. 5. Period T of the peak oscillations around the zero level in units of the driving period time T_{D} as function of the static field H_0 and the alternating field ΔH. For medium driving frequency $f_{\mathrm{D}} = 13$ Hz the calculated dynamics (a) shows harmonic, subharmonic and chaotic response in agreement with the experimental data (b). The measured critical field $H_{\mathrm{c}} = 6.2 \times 10^3\,\mathrm{A\,m^{-1}}$ was the same as in the static case. Thus we suppose that the susceptibility of the ferrofluid was $\chi = 2.93$.

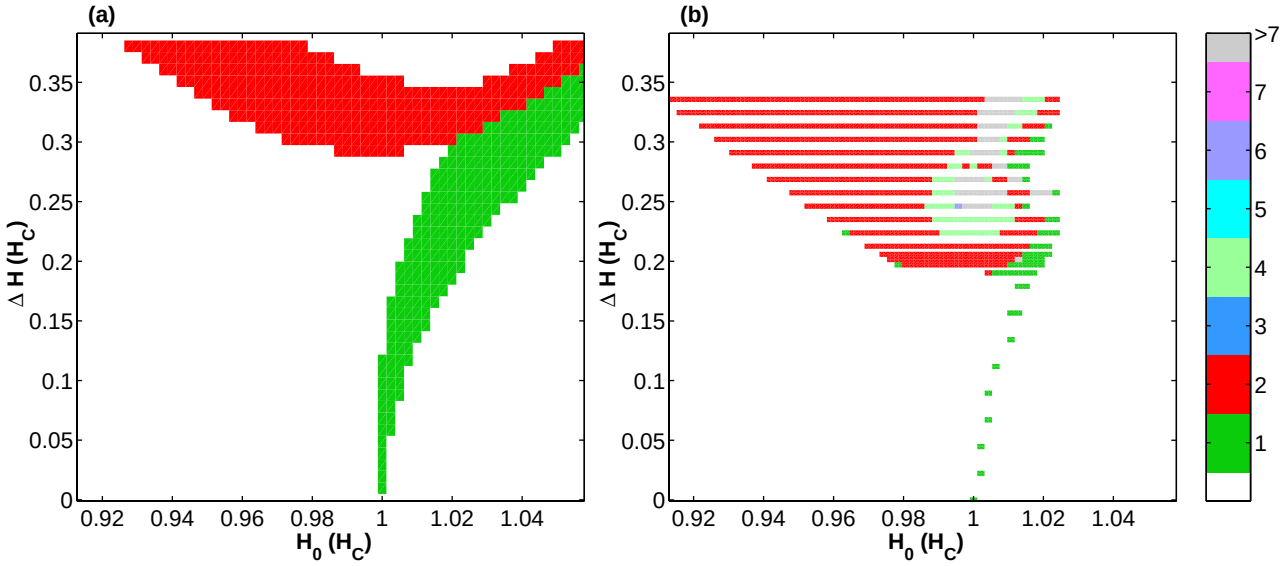

Fig. 7. Period T of the peak oscillations around the zero level in units of the driving period time T_{D} as function of the static field H_0 and the alternating field ΔH. For high driving frequency $f_{\mathrm{D}} = 23.5$ Hz in the simulation (a) only period-1-states and period-2-states are observed, while the measured dynamics (b) shows states with higher periods and intermittency.

7 Summary

We used the thermodynamic potential $\tilde{F}$ to analyse both the statics and the dynamics of the single ferrofluid peak. By minimizing this free energy we have determined the static shape of the peak. Our results for the subcritical bifurcation are in very good agreement with the experimental data.

Interpreting the derivative of $\tilde{F}$ with respect to the peak height h as a force we have deployed a model for the dynamics of the fluid peak. Applying this model we have qualitatively reproduced all essential features of the complex peak oscillations for the entire experimentally investigated spectrum of driving frequencies. For medium and high frequency a subharmonic response with periods up to 7 and 2, respectively, was observed, with the transition to higher periods happening *via* period doubling

or intermittence. A very good quantitative accordance with the experiment was achieved for low and medium frequencies. Our model should be applicable also to oscillations excited by vibrations of the solid base [16,17]. In the latter case and for high frequency it might be necessary to extend the proposed one-dimensional differential equation to a system of equations for more free parameters to get the same agreement. The phenomenological introduction of the inertia and the damping can probably only be improved by the calculation of the corresponding flow field of the ferrofluid. In the one-dimensional case this can again be done perturbatively [21]. For the two-dimensional situation a numerical simulation using finite elements is currently under way.

We thank Thomas Mahr and Ingo Rehberg for providing the experimental data and several interesting discussions. Special thanks are due to Alexander Rothert and Reinhard Richter for a careful measurement of the surface tension and the susceptibility respectively of the used ferrofluids. This work was supported by the *Deutsche Forschungsgemeinschaft* under the project En 278/2-1.

References

1. R.E. Rosensweig, *Ferrohydrodynamics* (Cambridge University Press, Cambridge, 1985).
2. E. Blums, A. Cebers, M.M. Maiorov, *Magnetic fluids* (de Gruyter, Berlin, New York, 1997).
3. W. Luo, T. Du, J. Huang, Phys. Rev. Lett. **82**, 4134 (1999).
4. J.P. McTague, J. Chem. Phys. **51**, 133 (1969).
5. M.I. Shliomis, Sov. Phys. JETP **34**, 1291 (1972).
6. M. Liu, Phys. Rev. Lett. **74**, 4535 (1995).
7. S. Odenbach, J. Magn. Magn. Mater. **201**, 149 (1999).
8. B. Berkovski, V. Bashtovoy, *Magnetic fluids and application handbook* (Begell House, New York, 1996).
9. T. Mahr, I. Rehberg, Physica D **111**, 335 (1998).
10. M.D. Cowley, R.E. Rosensweig, J. Fluid Mech. **30**, 671 (1967).
11. A. Gailitis, J. Fluid Mech. **82**, 401 (1977).
12. A.G. Boudouvis, J.L. Puchalla, L.E. Scriven, R.E. Rosensweig, J. Magn. Magn. Mater. **65**, 307 (1987).
13. A.G. Boudouvis, L.E. Scriven, J. Magn. Magn. Mater. **122**, 254 (1993).
14. A. Lange, H. Langer, A. Engel, Physica D **140**, 294 (2000).
15. A. Engel, H. Langer, V. Chetverikov, J. Magn. Magn. Mater. **195**, 212 (1999).
16. T. Mahr, A. Groisman, I. Rehberg, J. Magn. Magn. Mater. **159**, L45 (1996).
17. S. Sudo, M. Ohaba, K. Katagiri, H. Hashimoto, J. Magn. Magn. Mater. **122**, 248 (1993).
18. L.D. Landau, E.M. Lifshitz, *Elektrodynamik der Kontinua* (Akademie-Verlag, Berlin, 1974).
19. Note that these values differ from those mistakenly given in [9]. Recent measurements [20] on the same ferrofluid mixture as used in [9] however gave the results $\rho g = 1.35 \times 10^4\ \mathrm{kg\,m^{-2}\,s^{-2}}$, $\sigma \approx 2.20 \times 10^{-2}\ \mathrm{kg\,s^{-2}}$ and $\chi = 2.34...3.24$ depending on the age of the fluid. These measurements are in close agreement with the values of our fit.
20. R. Richter, A. Rothert (private communication).
21. G. Danker, Diploma thesis, Otto-von-Guericke-University Magdeburg, 1999.